ARTICLE

Effect of Laser Heat Input on Microstructure and Fatigue Behavior of TC17 Titanium Alloy Laser Welded Joint

Ren Lina[1,2], Zhang Qunbing[3], Lei Xiaowei[4], Qi Liang[2], Yang Jiadian[5], Zhang Jianxun[1]

[1] State Key Laboratory for Mechanical Behavior of Materials, Xi`an Jiaotong University, Xi`an 710049, China; [2] Western Titanium Technologies Co., Ltd, Xi`an 710201, China; [3] School of Materials Engineering, Xi`an Aeronautical Institute, Xi`an 710077, China; [4] School of Physical Science and Technology, Northwestern Polytechnical University, Xi`an 710072, China; [5] Guizhou Aviation Technical Development Co., Ltd, Guiyang 550081, China

Abstract: TC17 titanium alloy was weld under different laser heat input conditions. Optical microscope, scanning electron microscope, transmission electron microscope, tensile and fatigue tests were used to compare the macroscopic morphologies, microstructures, and mechanical properties of the welded joints. The results show that with the increase in heat input, the morphology of weld changes from Y- to X-shaped. The number of pore defects in the weld increases first and then decreases. The pore defects are mainly distributed in the middle and lower part of the weld zone. The weld is composed of coarse columnar grains with strip dendrites inside, and the spacing of dendrite increases gradually with the increase in heat input. The heat affected zone comprises finer equiaxed grains, and the increase in heat input leads to the refinement of α phase and coarsening of β phase. Moreover, the TC17 laser welded joints all fracture at the weld zone in the tensile and fatigue tests. Under the influence of dendrite size, the tensile strength decreases with the increase in heat input. The welding pore is the main reason for the fatigue fracture, and the fatigue life peaks when the number of pore defect is the lowest.

Key words: TC17 titanium alloy; welded joint; laser heat input; microstructure; fatigue behavior

Titanium alloys are widely used in advanced aerospace due to their high specific strength and excellent corrosion resistance. To reduce the mass of the aircraft, more and more titanium alloys are connected by welding.

TC17 is an $\alpha + \beta$ dual-phase titanium alloy with high strength[1-2], good toughness, high hardenability, good fatigue performance[3], and other advantages, so it is widely used in manufacturing aero-engine fans, integral blades, and other components[4-5]. At present, the welding of TC17 is mainly focused on electron beam welding and friction welding. Liu et al[6] investigated the microstructure and fatigue behavior of TC17 electron beam welded joint. They found that welding pores appear in the weld zone (WZ), and the microhardness of the WZ is lower than that of the base metal (BM)[7]. With the decrease in loading stress, the main cause of fatigue fracture gradually changes from inherent defects of WZ to porosity defects[8-9]. Xu et al[10] explored the internal tensile

deformation of the BM, heat-affected zone (HAZ), and WZ of TC17 electron beam welded joint. The microstructural evolutions in the HAZ and WZ decrease their mechanical properties. The needle-shaped thermal martensite formed during electron beam welding causes the WZ to fail prematurely. Song et al[11-12] studied the microstructures and fatigue properties of TC17 friction stir welded joint. Uneven microstructure is found in the solder stirring zone and HAZ. The fatigue crack growth rate of the HAZ is higher than that of the stirring zone. The fatigue crack initiation position of the welded joint changes with the variation of stress, i. e., the crack is initiated at the stirring zone at low amplitude stress, but generated at the HAZ at high amplitude stress. Zhao et al[13] investigated the heat treatment and fatigue properties of TC11 and TC17 linear friction welded joint. It is found that the impact toughness of the joint can be increased by 200% via annealing+solution+aging treatment. During the cyclic

deformation process, dislocation pile-up and stress concentration occur at the boundaries of the coarsened β phases, resulting in the fatigue fracture of the welded joint at the WZ on the TC17 side[14]. Wang et al[15] explored the corrosion properties of TC15 and TC17 linear friction welded joints. The high fraction of α/β phase interface in TC17 leads to poor corrosion resistance. The corrosion resistance of TA15 is better than that of TC17. After immersion and salt spray tests, a large number of corrosion pits form at the TC17 side of the WZ. Shen et al[16] studied the microstructure and fatigue properties of TC17 fabricated by laser direct energy deposition. The α phase laths in laser directly-deposited TC17 are fine and the size distribution is uniform, while α_p in wrought microstructure is coarse accompanied by nano-scale α_s in the β matrix. The total strain range of 2.0% is the minimum strain for cyclic softening of TC17 produced by laser direct deposition, otherwise, cyclic hardening will occur. When cyclic hardening occurs, the stress amplitudes of the two specimens are similar, but the stress amplitude of the laser directly-deposited specimen is smaller than that of the wrought specimen during the cyclic softening process. Wang et al[17] investigated the fatigue properties of laser additively-repaired TC17. The laser repaired columnar crystal is up to 200 μm. The microhardness of the WZ and HAZ decreases slightly, but the fatigue limit of the laser additively-repaired TC17 samples is significantly lower than that of the forged material. This reduction is attributed to the high crack growth rate caused by the coarse grains and, more importantly, defects such as pores.

Compared with electron beam welding and friction welding, laser welding has the advantages of flexible processing ability, fast welding speed, small HAZ, easy to realize automation, etc, and it has become one of the most efficient welding methods with rapid development in recent years[18–19]. However, the pore defects and coarse columnar grains are usually observed in the titanium alloy laser welded joints, which severely restrict the engineering application of titanium alloy[20]. When the laser power density is high enough to vaporize titanium alloy, a keyhole shape melt pool will be created[21]. In the keyhole laser mode, the fraction of the beam absorbed by the specimen is high (high coupling efficiency), leading to the high penetration depth as well as small HAZ and WZ. However, the keyhole is not at an ideal state of equilibrium, and owing to the periodic collapse and opening, pore defects tend to form in the weld[22]. Sun et al[20] studied the porosity of Ti-6Al-4V laser welded joints, and found that the porosity rate reaches 5.32% under the atmospheric pressure without beam oscillation. In contrast, the weld porosity decreases to 0.74% and 1.67% in the sub-atmospheric pressure (5 kPa) environment and laser oscillation, respectively. Kumar et al[23] found that the presence of pores in the WZ of the Ti6Al4V laser-welded joints lowers the tensile strength, and the size of the pores increases with the increase in heat input. Meanwhile, the pores generated during the welding process remain a crucial factor influencing the fatigue properties of welded joints[24]. Chattopadhyay et al[25] found

that the fatigue performance of laser beam welded commercially pure titanium is connected with the internal pores within the WZ, and the pores act as stress concentration points, leading to shorter fatigue life.

The weld microstructures of titanium alloys formed under different laser welding conditions is very different, which will affect the comprehensive properties of welded joints distinctly[26]. For instance, Li et al[27] studied the effect of laser welding parameters on microstructure and properties of 3 mm-thick TC4 titanium alloy. The experimental results indicate that laser welding parameters such as laser power, welding speed, and defocus position have important influences on the microstructures of WZ and HAZ.

Clearly, the existing studies mainly focus on the effects of laser power and scanning rate on the microstructure and properties of welding joints, but the essence is the interaction of these two parameters, that is, the influence of heat input. Particularly, the design of heat input is crucial once the shape of weld zone changes significantly. However, relevant work on TC17 alloy is still insufficient, and further clarifications on the relationship among heat input, microstructure, and fatigue performance are indispensable. Therefore, in this research, laser welding was performed on TC17, and the effect of laser heat input on the microstructures and fatigue properties of the welded joint was studied. The research results can provide a meaningful reference for the regulation and control of the microstructure and mechanical properties of TC17 welded joints.

1 Experiment

1.1 Materials and welding

The BM was forged TC17 titanium alloy. As shown in Fig.1, its microstructure is primary α (α_p)+β dual-phase with an average grain size of about 4 μm, and large amounts of
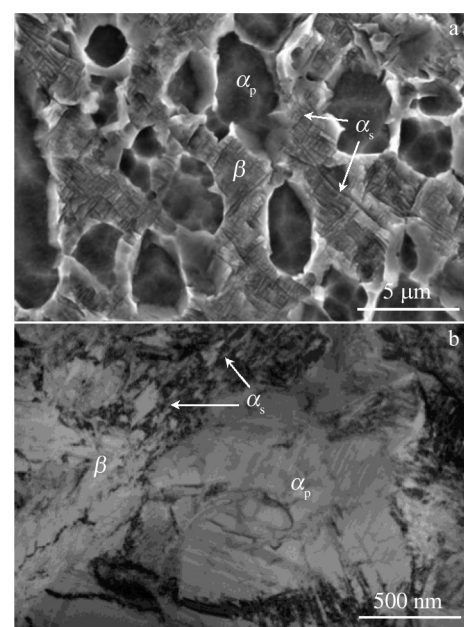
Fig.1　SEM (a) and TEM (b) images of TC17 BM

martensitic secondary α (α_s) phases are distributed in the β phase. The chemical composition of TC17 is shown in Table 1. The forged TC17 was cut into plates with 5 mm in thickness. The plates were then etched for 120 s by 90 mL pure water+6 mL HNO_3+4 mL HF to remove the surface stains. Finally, the surfaces of the plates were wiped with dehydrated ethanol and dried naturally. These treated specimens were immediately welded by YLS-4000 fiber laser with a YASKAWA welding robot. The schematic illustration of welding process and the welding parameters are shown in Fig.2a and Table 2, respectively.

1.2 Fatigue tests and microstructure characterizations

The specimens for tensile tests were prepared according to the standard ISO 4136: 2022, and the specimens for fatigue tests were prepared according to the standard ISO 12106: 2017. The welded plate was machined into tensile and fatigue samples by electrical discharge wire cutting equipment and grinding machine. The final specimen thickness was 3 mm. The schematics of the specimens are shown in Fig.2b and 2c.

Stress-controlled tensile-compressive fatigue tests were performed on electro-hydraulic fatigue machine. A triangular waveform was selected. As the yield strength of TC17 base metal is 1030 MPa, 900 MPa (about 90% of the yield strength) was chosen as the stress amplitude for the fatigue experiment. The stress ratio was $R = -1$, and the frequency was 0.125 Hz. Each tensile and fatigue experiment was repeated three times, and the average value was used as the experimental result. The laser heat input refers to Joule heat in a certain unit length during welding, so its unit in this research is J/mm. The laser heat input is affected by laser power and welding speed, and its calculation formula is as follows:

$$E = p/v \tag{1}$$

where E is laser heat input, p is laser power, and v is welding speed.

Microhardness tests were carried out by TMVS-1 micro-Vickers hardness tester. The indentation force was 2.94 N, and the loading time was 15 s. HIROX-200 ultra-depth field optical microscope (OM), JSM-6510A scanning electron microscope (SEM), and JEM-2100 transmission electron microscope (TEM) were used to analyze the macroscopic morphologies and microstructures of the welded joints and the fracture morphologies of the fatigue specimens.

2 Results and Discussion

2.1 Effect of laser heat input on weld morphology

The influence of laser heat input on the macroscopic morphologies of the welded joints is shown in Fig.3. With the increase in laser heat input, the cross-section morphology of the WZ changes from Y- to X-shaped. The width of the WZ increases, and the fusion line between the WZ and the HAZ becomes unclear gradually. The number of welding pores in the center of WZ increases and then declines.

The schematic diagrams of the Y- and X-shaped cross-section morphology of the welded joint are shown in Fig. 4. Due to the high energy density of laser, the weld metal vaporizes. When the laser heat input is low, a keyhole will form in the center of the molten pool. The depth of the keyhole is lower than the thickness of specimen. When the sum of depth of keyhole+the depth of the bottom of the molten pool is slightly higher than the thickness of specimen, the bottom of the molten pool will sink, resulting in the molten pool extruding from the bottom surface of specimen and forming the Y-shaped WZ, as shown in Fig.4a. When the laser heat input is large, the depth of the keyhole reaches or exceeds the thickness of specimen, suggesting that the molten pool is penetrated. The metal steam sprays out from the top
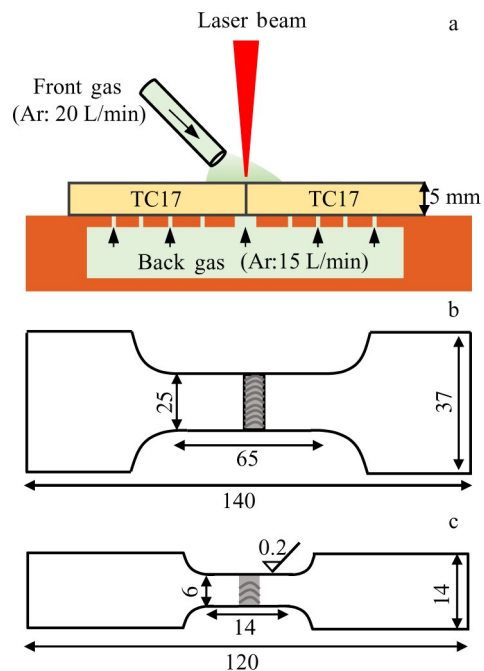
Fig.2 Schematic diagrams of welding process (a), tensile test specimen (b), and fatigue test specimen (c)

Table 1 Chemical composition of TC17 (wt%)

Al	Sn	Zr	Mo	Cr	C	Fe	O	Ti
5.15	1.98	2.01	3.83	3.80	0.020	0.024	0.10	Bal.

Table 2 Laser welding parameters

Specimen	Laser power/kW	Welding speed/mm·min⁻¹	Laser heat input/J·min⁻¹	Laser defocusing/mm	Shielding gas
1	3	90	2000		
2	3.5	90	2333		
3	3.5	80	2625	0	Ar (99.99%)
4	4	80	3000		
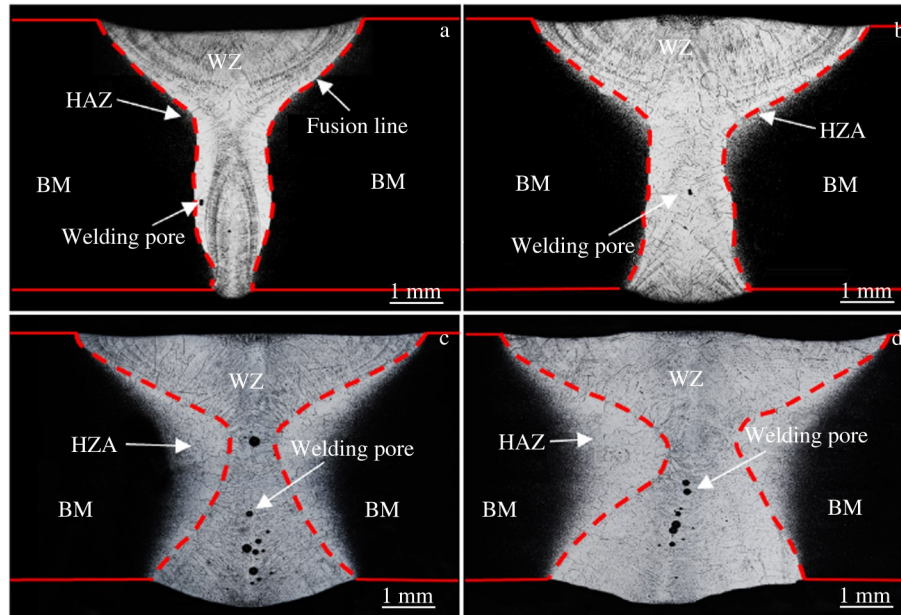
Fig.3　Effect of laser heat input on macroscopic morphologies of the welded joints: (a) 2000 J/mm, (b) 2333 J/mm, (c) 2625 J/mm, and (d) 3000 J/mm
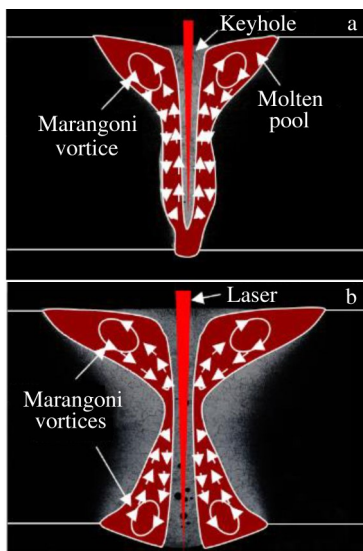
Fig.4　Schematic diagrams of Y-shaped (a) and X-shaped (b) morphologies of the welded joint

and bottom of the keyhole, driving the liquid metal to flow upward and downward along the keyhole wall, and thus leading to the formation of two relatively independent Marangoni vortices[28–29] on the top and bottom parts of the molten pool. As a result, the widths of the top and bottom of the molten pool are larger than that of the middle part. Then, the cross-section of the WZ will be X-shaped, as shown in Fig.4b.

It is precise that the difference in the liquid metal flow mode between Y- and X-shaped WZ that leads to the difference in the number of welding pores. During the post-weld cooling process, the molten pool solidifies in a short time due to the rapid cooling rate. For the Y-shaped WZ, liquid metal flows downward along both sides of the keyhole, the gas in the keyhole will escape upward, so there are few porosity defects after solidification, as shown in Fig. 3a and 3b. However, when the liquid metal of the upper part of X-shaped WZ flows downward, the bottleneck in the middle of the X-shaped WZ has a blocking effect on the liquid and gas flows. At the upper part of the WZ, the gas is discharged along the keyhole, while the gas at the lower part of the WZ cannot escape completely. Therefore, a large number of welding pores remain at the lower part of the X-shaped WZ, as shown in Fig. 3c and 3d. With the increase in heat input, the time required for solidification of WZ prolongs, and the time for upward escape of pores in the lower part of the WZ increases. In addition, the increase in heat input leads to lower viscosity of the melt zone, which also favors the escape of gas. Therefore, for X-shaped WZ, the number of pores decreases with the increase in heat input, as shown in Fig.3c and 3d.

2.2 Effect of laser heat input on microstructure

During the welding process, although the region out of the edge of the molten pool does not melt, the temperature will exceed the phase transition point of α_p and α_s, and the grain size will be enlarged, as shown in Fig.5. At the same time, all the martensitic α_s in the β in this region disappears, and with the increase in laser heat input, the α_p is gradually transformed into β, rendering the microstructure close to a pure β phase. The average grain size of β phase of the BM is about 4 μm (Fig.1). In contrast, when the welding heat input is low (2000 J/mm), the average grain size of the HAZ is about 6 μm (Fig. 5a). With further enhancing the laser heat input, the average grain size of the HAZ increases to 10 μm gradually (Fig. 5b–5d).

Fig. 3 shows that the WZ of TC17 laser welded joint is
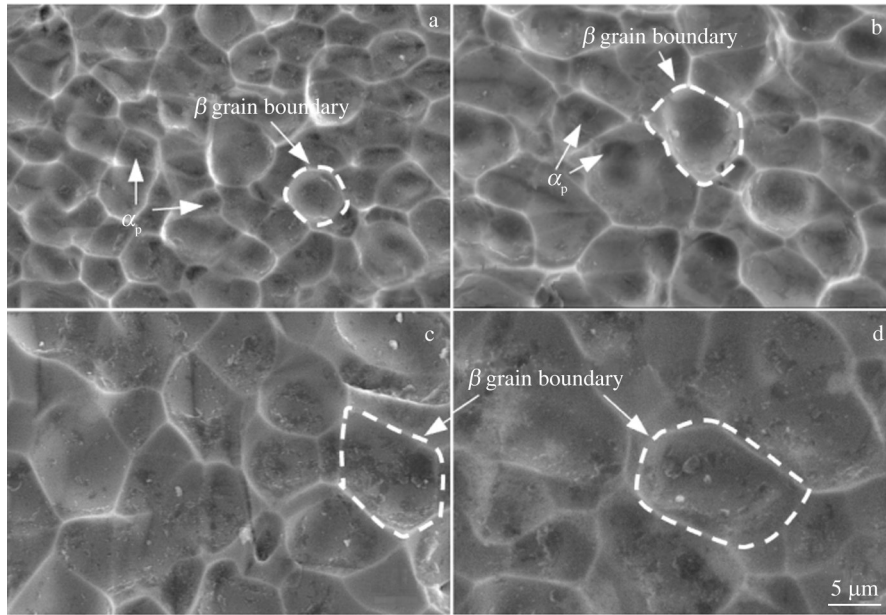
Fig.5   Effect of laser heat input on the microstructures of HAZ: (a) 2000 J/mm, (b) 2333 J/mm, (c) 2625 J/mm, and (d) 3000 J/mm

mainly composed of columnar crystals, so the impact of laser heat input on the morphologies of the columnar crystals was analyzed. The microstructure of the WZ (Fig. 6) reveals that the columnar crystals mainly comprise neatly arranged dendrites. When the laser heat input is 2000 J/mm, the average spacing between dendrites is about 6 μm (Fig. 6a). With the increase in the laser heat input, the average spacing between the dendrites gradually increases to about 13 μm (Fig.6d). The main reason for this phenomenon is that with the increase in laser heat input, the heat in the molten pool increases, the heat dissipation time will be extended, and thereby, the growth time of dendrites is extended, leading to increased dendrite spacing[30].

Fig. 7 shows the microstructures at the fusion lines under different laser heat inputs. It can be seen that when the laser heat input is 2000 J/mm, a clear boundary is formed between the HAZ and the WZ (Fig.7a). This is because when the laser heat input is low, the microstructure of the HAZ is $\alpha_p+\beta$ dual-phase, but the WZ consists of β phase, so there is a significant difference in the microstructure between HAZ and WZ. With the increase in laser heat input, the α_p phase in the HAZ is gradually transformed into β phase, and the grain size of the β phase increases. Meanwhile, with the increase in heat input, the movement and annexation of β phase boundary become
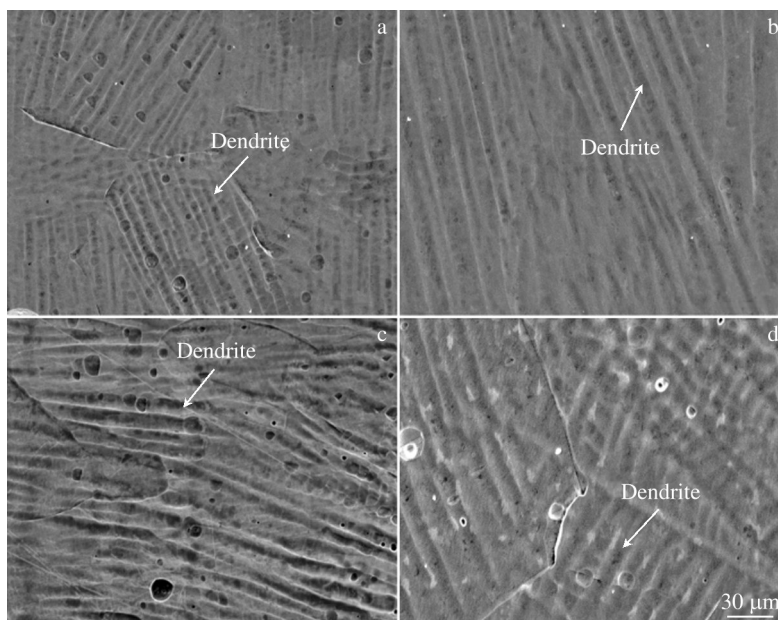
Fig.6   Effect of laser heat input on the microstructures of the WZ: (a) 2000 J/mm, (b) 2333 J/mm, (c) 2625 J/mm, and (d) 3000 J/mm
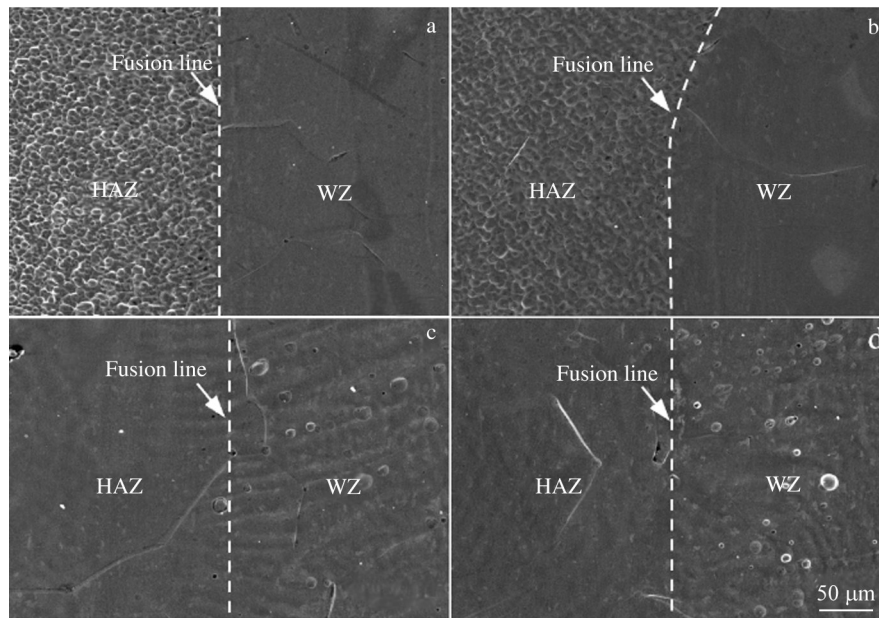
Fig.7 Effect of laser heat input on microstructures at the fusion lines: (a) 2000 J/mm, (b) 2333 J/mm, (c) 2625 J/mm, and (d) 3000 J/mm

more and more obvious. Therefore, the larger the laser heat input, the more similar the microstructures of the HAZ and WZ, leading to the unclearness of the fusion line (Fig.7b–7d).

Different microstructures of the BM, HAZ, and WZ lead to different mechanical properties. As can be seen from the microhardness curve of the welded joint (Fig. 8), the microhardness decreases from the BM to the WZ.

In general, the smaller the grain size, the stronger the grain boundary strengthening effect. As mentioned above, the microstructure distribution of BM, HAZ, and WZ are $\beta+\alpha_p+\alpha_s$ (Fig. 1), $\beta + \alpha_p$ (Fig. 5), and columnar β phases (Fig. 6),
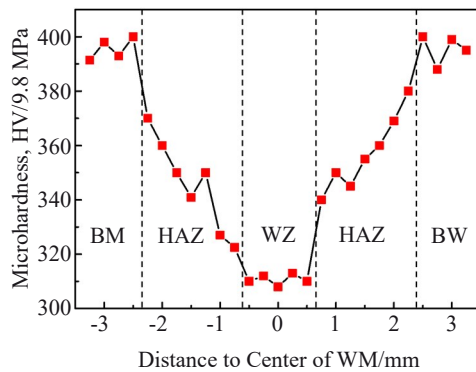
Fig.8 Microhardness curve of TC17 welded joint under laser heat input of 2625 J/mm

respectively. The average grain size of the BM, HAZ, and WZ gradually increases, resulting in a decrease in microhardness. Meanwhile, crystal structures of α_p and α_s are close-packed hexagonal (hcp) type, and the crystal structure of β is body-centered cubic (bcc) type. As is known, there are 12 slip systems for bcc crystal and 3 slip systems for hcp crystal. The more the slip systems, the better the plasticity, so the plasticity of β is better than that of α_p and α_s[31]. Therefore, from BM to HAZ and then to WZ, the microhardness gradually decreases.

2.3 Effect of laser heat input on fatigue behavior

Table 3 shows the tensile and fatigue test results of the welded joints under different laser heat inputs. All the tensile and fatigue specimens are fractured at the WZ. Moreover, with the increase in laser heat input, the tensile strength of the welded joint decreases gradually, but the fatigue life increases, then decreases, and increases again.

As shown in Fig.6, with the increase in laser heat input, the space between dendrites inside the WZ gradually increases from 6 μm to 13 μm. According to the Hall-Petch relationship[32]:

$$\sigma_y = \sigma_0 + K \cdot d^{-\frac{1}{2}} \qquad (2)$$

where σ_y is yield strength, σ_0 is friction stress (or yield strength of a single crystal), K is Halle-Petch slope, and d is grain size. K was reported to depend on the type and concentrations of interstitial alloying element. So, the strength

Table 3   Tensile and fatigue test results of welded joints under different laser heat inputs

Laser heat input/J·mm⁻¹	Tensile strength/MPa	Tensile fracture position	Fatigue life/cycle	Fatigue fracture position
2000	982	WZ	473	WZ
2333	968	WZ	518	WZ
2625	949	WZ	444	WZ
3000	942	WZ	513	WZ

of the materials will be reduced with the increase in dendrite spacing d. Combining the average dendrite spacing of the WZ (Fig. 6) and the tensile strength of the welded joint (Table 3), as shown in Fig. 9, with the increase in laser heat input, the average dendrite spacing of the WZ increases, leading to declined tensile strength, which is in good agreement with the Hall-Petch relationship.

Fig. 10 shows the fatigue fracture morphologies of the welded joint. Fig. 10a and 10e show the macroscopic feature of the fatigue fracture surface. It can be seen that there are many welding pores. As shown in Fig. 10b and 10f, some welding pores also exist in the fatigue crack initiation zone. In the enlarged images (Fig. 10c and 10g) of the fatigue crack initiation position of the crack initiation zone, there is welding pore too. In the fatigue crack growth zone (Fig. 10d and 10h), it can be seen that there are wave-like fatigue stripes perpendicular to the direction of crack growth, indicating that the plasticity of the WZ is good.
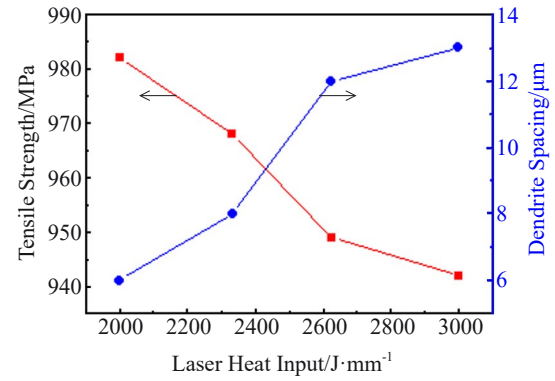
Fig.9 Effect of laser heat input on dendrite spacing and tensile strength of TC17 welded joint

Fig. 10 reveals that the welding pore is the main reason for the fatigue fracture of the welded joint. Fig. 11 shows the relationship between the number of welding pores (Fig. 3) and
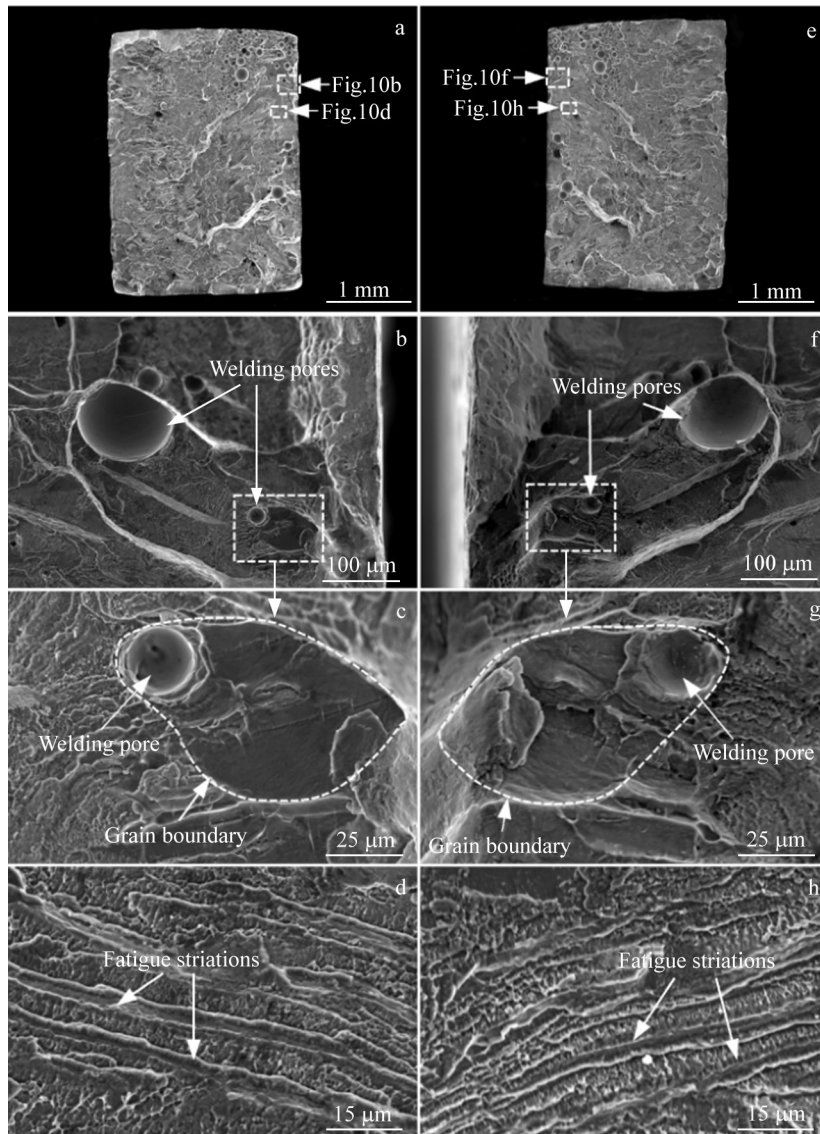
Fig.10 Fatigue fracture morphologies of TC17 welded joint under laser heat input of 2625 J/mm: (a, e) macroscopic feature; (b, f) fatigue crack initiation zone; (c, g) enlarged image of the fatigue crack initiation zone; (d, h) fatigue crack growth zone
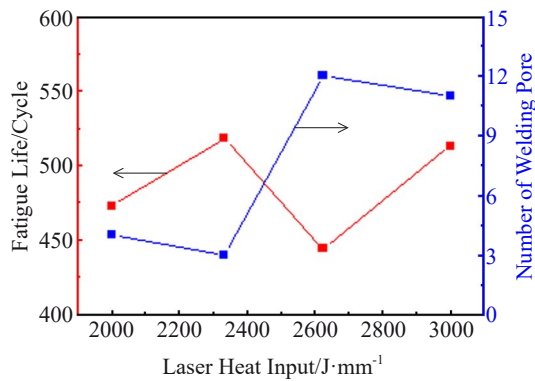
Fig.11 Effect of laser heat input on the number of welding pores and fatigue life of TC17 welded joint

fatigue life (Table 3). Clearly, the number of welding pores is completely negatively related to the fatigue life, i.e., the more the welding pores, the shorter the fatigue life of the welded joint. The lowest fatigue cycle locates at the specimen welded with the laser heat input of 2625 J/mm, where the WZ exhibits X-shaped morphology, evidencing the detrimental effect of pore trapping during the formation of X-shaped WZ. Meanwhile, the fatigue performance of the weld is affected by multiple factors, not only the number of pores, but also the microstructure of the WZ. When the heat input is high, the dendrite spacing of WZ is large. It will reduce the strength but improve the plasticity of the weld, and the fatigue life will be improved. So, although the number of pores is higher when the heat input is 3000 J/mm, the fatigue cycle is also improved to some extent due to the increase in the dendrite spacing.

3 Conclusions

1) With the increase in laser heat input, the macro morphology of the WZ changes from Y-shaped to X-shaped. Lots of welding pores form at the lower part of the X-shaped WZ.

2) From BM to HAZ and them to WZ of the welded joint, the microhardness decreases gradually. With the increase in laser heat input, the tensile strength of the welded joint decreases gradually, which is mainly due to the increased dendrite spacing and the declined number of dendrites in the WZ.

3) The fatigue fracture position of the welded joint locates at the WZ, and the main reason for the fatigue fracture is the welding pores. With the increase in the laser heat input, the fatigue life of the welded joint increases, then decreases, and increases again. The fewer the welding pores, the longer the fatigue life of the welded joint.

References

1 Yang C, Liu Y G, Shi Y H *et al. Materials Science and Engineering A*[J], 2020, 784: 139298

2 Li Ju, Chang Chuanchuan, Li Xiaohong *et al. Rare Metal Materials and Engineering*[J], 2022, 51(3): 940 (in Chinese)

3 Guo Ping, Pan Hao, Jia Guoyu *et al. Rare Metal Materials and Engineering*[J], 2022, 51(1): 301 (in Chinese)

4 Pang H Y, Liu Y G, Luo J *et al. Journal of Materials Science & Technology*[J], 2023, 157: 246

5 Yu Y B, Yan H G, Chen J H *et al. Journal of Alloys and Compounds*[J], 2022, 912: 165260

6 Liu H Q, Song J, Wang H M *et al. International Journal of Fatigue*[J], 2022, 154: 106525

7 Liu H Q, Wang H M, Zhang Z *et al. International Journal of Fatigue*[J], 2019, 128: 105210

8 Liu F L, Chen Y, He C *et al. International Journal of Fatigue*[J], 2021, 152: 106446

9 Liu F L, Chen Y, Li L *et al. Journal of Materials Science & Technology*[J], 2024, 178: 1

10 Xu C, Liu H Q, Li C H *et al. Materials Science and Engineering A*[J], 2023, 875: 145087

11 Song J, Liu H Q, Tan K *et al. Materials Science and Engineering A*[J], 2021, 822: 141694

12 Song J, Liu H Q, Cui J *et al. International Journal of Fatigue*[J], 2023, 168: 107426

13 Zhao P, Wei C, Li Y *et al. Materials Science and Engineering A*[J], 2021, 803: 140496

14 Zhao P, Fu L, Chen H. *Journal of Alloys and Compounds*[J], 2016, 675: 248

15 Wang C, Guo Q, Shao M *et al. Materials Characterization*[J], 2022, 187: 111871

16 Shen S, He B, Wang H. *Materials Science and Engineering A*[J], 2024, 890: 145883

17 Wang L, Luo S, Lu K *et al. International Journal of Fatigue*[J], 2024, 178: 108026

18 An F, Liu X, Zhang H *et al. Optics & Laser Technology*[J], 2024, 170: 110256

19 Lei Xiaowei, Liu Jia, Yu Wei *et al. Rare Metal Materials and Engineering*[J], 2024, 53(2): 417 (in Chinese)

20 Sun H, Xu B, Li R *et al. Journal of Materials Research and Technology*[J], 2024, 29: 4245

21 Rominiyi A L, Mashinini P M. *Journal of Advanced Joining Processes*[J], 2024, 9: 100191

22 Li J M, Jiang P, Geng S N *et al. International Journal of Heat and Mass Transfer*[J], 2023, 214: 124443

23 Kumar P, Sinha A N. *Welding in the World*[J], 2018, 63(3): 673

24 Liu F, Chen Y, Li L *et al. Journal of Materials Science & Technology*[J], 2024, 178: 1

25 Chattopadhyay A, Muvvala G, Sarkar S *et al. Optics & Laser Technology*[J], 2021, 133: 106527

26 Ai Y, Wang Y, Yan Y *et al. Optics & Laser Technology*[J], 2024, 170: 110195

27 Li G, Wang Y, Liang Y *et al. Optics & Laser Technology*[J], 2024, 170: 110320

28 Huang W, Wang H, Rinker T *et al. Materials & Design*[J], 2020, 195: 109056

29 Liu L, Wang G, Ren K *et al. Additive Manufacturing*[J], 2022, 59: 103156

30 Ai Y, Han S, Yan Y. *Thermal Science and Engineering Progress*[J], 2024, 47: 102259

31 Paes V Z C, Mosca D H. *Journal of Magnetism and Magnetic Materials*[J], 2013, 330: 81

32 Park S J, Kim K S, Kang J H *et al. Journal of Materials Research and Technology*[J], 2022, 19: 2960

激光线能量对TC17钛合金焊接接头组织和疲劳性能的影响

任利娜[1,2]，张群兵[3]，雷晓维[4]，齐　亮[2]，杨家典[5]，张建勋[1]

(1. 西安交通大学　金属材料强度国家重点实验室，陕西　西安　710049)

(2. 西部钛业有限责任公司，陕西　西安　710201)

(3. 西安航空学院　材料工程学院，陕西　西安　710077)

(4. 西北工业大学　物理科学与技术学院，陕西　西安　710072)

(5. 贵州航宇科技发展股份有限公司，贵州　贵阳　550081)

摘　要：在不同的激光线能量条件下对TC17钛合金进行了焊接，采用光学显微镜、扫描电镜、透射电镜、拉伸和疲劳试验机对接头的宏观形貌、微观组织和力学性能进行了对比研究。结果表明：随着激光线能量的增加，焊缝宏观形貌由Y型转变为X型、焊缝中气孔缺陷数量先增加后减少，气孔缺陷主要分布在焊缝的中下部。焊缝由柱状晶粒组成，柱状晶内部存在条形枝晶，枝晶间距随着线能量的增加而逐渐增大。热影响区由尺寸较小的等轴晶组成，随着激光线能量的增加，α相晶粒逐渐细化，而β相逐渐粗化。在拉伸和疲劳试验中，TC17激光焊接接头均断裂在焊缝。受焊缝内部枝晶尺寸的影响，抗拉伸强度随线能量的增加而降低。气孔是导致疲劳断裂的主要原因，气孔缺陷数量越少，则疲劳寿命越长。

关键词：TC17钛合金；焊接接头；激光线能量；微观组织；疲劳行为

作者简介：任利娜，女，1980年生，博士，正高级工程师，西安交通大学金属材料强度国家重点实验室，陕西　西安　710049，E-mail：ren.lina@hotmail.com